SyncSci PUBLISHING

Chem Rep, 2022, 4(1): 244-255
DOI: 10.25082/CR.2022.01.003

RESEARCH ARTICLE

Fabrication of Pb_3O_4 and Fe_2O_3 nanoparticles and their application as the catalysts in thermal decomposition of ammonium perchlorate

Hossein Momenizadeh Pandas[1] **Mostafa Fazli**[1*]

[1] Chemistry Department, Faculty of Science, Semnan University, Semnan, 35195-363, Iran

Check for updates

Correspondence to: Mostafa Fazli, Chemistry Department, Faculty of Science, Semnan University, Semnan, 35195-363, Iran; E-mail: mfazli@semnan.ac.ir

Received: July 11, 2022;
Accepted: September 3, 2022;
Published: September 7, 2022.

Citation: Pandas HM and Fazli M. Fabrication of Pb_3O_4 and Fe_2O_3 nanoparticles and their application as the catalysts in thermal decomposition of ammonium perchlorate. *Chem Rep*, 2022, **4**(1): 244-255. https://doi.org/10.25082/CR.2022.01.003

Copyright: © 2022 Hossein Momenizadeh Pandas *et al*. This is an open access article distributed under the terms of the Creative Commons Attribution License, which permits unrestricted use, distribution, and reproduction in any me- dium, provided the original author and source are credited.

Abstract: Nanoparticles (NPs) of lead tetroxide (Pb_3O_4) with the spherical morphology were manufactured by the reaction of lead nitrate with sodium hydroxide, while the nanoparticles (NPs) of red iron oxide (Fe_2O_3) with similar morphology were fabricated by hydrothermal route in the presence of ferric chloride hexahydrate as the precursor. Evaluation of the chemical structure, the purity and the morphology of the manufactured Fe_2O_3 and Pb_3O_4 NPs was carried out by analysis via X-ray diffraction (XRD) as well as scanning electron microscope (SEM). The outcomes of XRD recognized establishment of the desired oxides, wherever the SEM images clearly exhibited the morphology of the manufactured $Pb_3O_4$and Fe_2O_3 as the spherical NPs with an average particle sizes of near to 40 and 46 nm, respectively. The catalytic effect of the metallic oxide NPs on the perfection of ammonium perchlorate (AP) thermal decomposing was established by testing their AP nano-composites via differential scanning calorimetric (DSC) together with thermogravimetric analysis (TG). Thermal behavior studies displayed that adding of 5% Fe_2O_3/Pb_3O_4 NPs (as the mixture) delivers a concerned catalytic effect during AP thermal decomposition. Additionally, thermal decomposition of AP could be amended by adding of 2% Pb_3O_4 NPs. Further comparison of the NPs catalytic effects was obtained by computing the values of activation energies (*E*) and thermodynamic parameters (*i.e.*, $\Delta S^{\#}$, $\Delta H^{\#}$ and $\Delta G^{\#}$) for their thermal decomposition by non-isothermal approaches.

Keywords: lead tetroxide, iron oxide, nanoparticles, ammonium perchlorate (AP), nano-catalyst effect, thermal decomposition, kinetics and thermodynamic factors

1 Introduction

Ammonium perchlorate (AP) has been employed in various propellant formulations as a substantial oxidant [1, 2]. The thermal pattern of ammonium perchlorate containing three successive events has been discussed in the literature [3–6]. The thermal properties of AP is important, because it has a remarkable impact on the combustion characteristics of the propellants containing AP. Some unfavorable combustion properties of the pure AP including low decomposition energy along with relative high decomposition temperature limit its applications. Nonetheless, these characteristics could be improved somewhat by its treating with some catalysts [5–7]. Sensitivity of AP particles to different additives is a precise property which influences on its thermal decomposition. These additives in homogeneous or heterogeneous mixtures may either inhabit or promote AP particles decomposition [7]. Up to now, several classes of nano-materials comprising oxides of metals [8–13], the mixture of metal oxides [14–16], and further kinds of nano-materials have been utilized as the nano-catalyst for elevation of AP thermal decomposition and some of them showed substantial catalytic effects. In fact, AP particle size reduction may yields similar results, nonetheless the high reactivity of superfine particles of AP could be possibly unsafe [17]. Consequently, numerous investigations have been directed toward combination of different NPs to AP in place of functioning risky and abandoned reactions [7].

Iron oxide in the nature could be found in three forms comprising Fe_3O_4 (magnetite), γ-Fe_2O_3(maghemite) and α-Fe_2O_3(hematite). The latter form is the oldest known type of iron oxide which has numerous applications, particularly as the catalyst, due to its abundance, high stability, cost-effectiveness, and non-toxicity [18–26]. Various routes have been applied previously to prepare nanoparticles of iron oxide in the form of hematite (α-Fe_2O_3). The most applied method is the hydrothermal process due to its facile manipulation, scalable preparation and precise control of the product size [27].

Lead oxides (four basic forms, *i.e.* PbO, PbO_2, Pb_2O_3 and Pb_3O_4) possess unique properties, which caused their widely applications for instance network-modifiers in the luminescent glassy compositions, storage batteries, pigments, and nano-electronic devices [28]. The binary lead oxides are seem as infrequent topic and only a few other metal oxides are similar to them

that exist as complex which makes this group of compounds interesting. Some members of lead oxides are belonging to the class of conducting metal oxides and hence they have a wide range of applications in the electronic fields. Lead oxides have also other applications *i.e.* as a direct conversion material in the X-ray imaging detectors [29] and as the transparent conducting films [30] which exhibit the optical transmission in the visible region and reflectance in infrared section of electromagnetic spectrum. Due to their unique electronic properties and also ability to their fabrication in various forms by a diversity approaches, they have a great potential for utilizing in many more fields in the future. Moreover, their combining with other materials may effortlessly result in many more claims as composites [31].

During recent decades, thermal analysis techniques have been applied for compatibility studies of diverse materials. Correspondingly, thermo-kinetic studies have been developed as a core in thermal analysis researches, in which fortitude of the pyrolysis reaction mechanism and also calculation of the Arrhenius parameters are the main purposes. This information is mandatory for the energetic materials to be experienced for performance and safety throughout their production, treatment, stowage and use [32]. In this study, the special effects of manufactured Pb_3O_4 and Fe_2O_3 NPs on the thermal behavior of ammonium perchlorate (AP) particles were appraised analytically by TG/DSC analysis under an inert atmosphere. Then, the thermo-kinetic parameters of the decomposition reaction, *i.e.*, activation energies were calculated by well-known non-isothermal methods of Kissinger and Starink.

2 Experimental

2.1 Materials

NH_4ClO_4 particles the average size nearby 80-100 μm as the powder with the laboratory grade purity as well as reagent grade ferric chloride hexahydrate, sodium hydroxide, urea, glycine, and lead nitrate were acquired from the Merck Company (Germany) and used as received. MIBK or methyl isobutyl ketone (purity $> 99\%$) was also purchased from the Merck Company (Germany). Besides, deionized water was used for the preparation of nano-composite samples.

2.2 Instrumentation

Manufactured NPs of Pb_3O_4 and Fe_2O_3 were evaluated by the scanning electron microscope (SEM model KYKY-EM3200, China), X-ray diffraction (XRD), and inductively coupled plasma (ICP model TY-9900, China) to characterize their chemical composition, structure and morphology of their particles. Before recording the SEM images, the AP samples were coated with a golden film. These films were organized by a sputter coater model SCD005 made by BAL-TEC (Switzerland). XRD analysis of the nano-materials was carried out on a Rigaku D/max 2500V diffractometer equipped with the Cu target and graphite as the monochromator. DSC and TG as the thermal analysis systems were applied to examine thermal behavior of the structured nano-composites. TG/DSC tests were performed on a Mettler TA4000 thermal analyzer coupled with a DSC (Mettler Toledo Co., Switzerland). While, further DSC examinations were carried out at the subsequent operational conditions: roughly 3 mg of the sample; purging of N_2 gas with 50 ml. min^{-1} flowing rate; an alumina crucible as the sample container; operating temperature at the range of 30 to 850°C by the side of the heating rates of 5, 10, 15, and 20°C.min^{-1}. Moreover, TG assessments were done at the subsequent operational situations: roughly 3 mg of the sample; an alumina crucible as the sample container; purging of N_2 gas with 50 ml. min^{-1}flowing rate; operating temperature at the range of 50 to 900°C by the side of the heating rates of 10°C.min^{-1}.

2.3 Synthesis of Fe_2O_3 nanoparticles

Red iron oxide (Fe_2O_3) NPs were synthesized by a simple hydrothermal route using ferric chloride hexahydrate ($FeCl_3{\cdot}6H_2O$) as the precursor. To begin with this process, 3.47 g of $FeCl_3{\cdot}6H_2O$ was added to 100 ml of the deionized water. The resulted mixture was stirred until the $FeCl_3{\cdot}6H_2O$ was completely dissolved in water; then, 1.55 g and 0.96 g respectively of urea and glycine were introduced to the mixture through stirring during 1 h. The prepared mixture was sealed in a Teflon-lined stainless-steel autoclave then kept up at 180°C for 24 h, and after that cooled naturally to the room temperature. The resultant product was then collected via centrifugation, and washed several times with the deionized water and ethanol and subsequently dried at 60°C.

2.4 Fabrication of Pb_3O_4 nanoparticles

Lead tetroxide was prepared by the reaction of a lead nitrate solution withsodium hydroxide solution. A concentrated solution of sodium hydroxide was obtained by dissolving 300 grams of the sodium hydroxide in distilled water, while the solution was heated during dissolving process. Then, the resulted solution was cool down to the room temperature. In the next step, 50 g lead

nitrate was dissolved in 200 ml of distilled water and slowly added to the sodium hydroxide solution while stirred continuously. During the formation process, at first a white precipitate was formed, which turned to the orange when whole of sodium hydroxide solution was added. After an hour stirring this solution, the lead tetroxide was deposited. Then, the lead tetra oxide was filtered and washed in the filter several times with the hot distilled water.

2.5 Organizing of the modified AP nano-composites

The catalytic activity of Pb_3O_4andFe_2O_3 NPs was inspected by preparing their nano-composites with the AP. Therefore, nano-composites of AP in the presence of diverse amounts (0.5, 2 and 5%w/w) of either Pb_3O_4 or Fe_2O_3+Pb_3O_4 NPs were prepared via solvent/ non-solvent mixing procedure as recommended formerly [31,32]. Water and MIBK correspondingly were utilized as the solvent and non-solvent of the AP. In order to prepare the nano-composites, the corresponding masses of NPs in 30.0 mL of MIBK (as the AP non-solvent) were dispersed thru their sonication in an ultrasonic bath for about 10 min. At that moment, to organize the saturated solution of AP, the related mass of AP was dissolved in 10.0 mL of warmed distilled water at temperature of 80 °C. Subsequently, the saturated AP solution was introduced drop by drop to the MIBK comprising dispersed NPs to form the precipitate AP+NPs as the nano-composite. In the next step, the precipitated AP nano-composite particles were filtered and subsequently washed three times with about 20 mL of the MIBK as non-solvent and last of all dried at the room environment.

3 Results and discussion

3.1 Manufacturing and characterizing of lead tetroxide and red iron oxide nanoparticles

The SEM images of synthesized metal oxides NPs are presented in Figure 1. As expected, the particles of the formed oxides exhibit a spherical morphology. The SEM images show that the mean sizes of the lead tetroxide and iron oxide particles are about 46 and 40 nm, respectively.

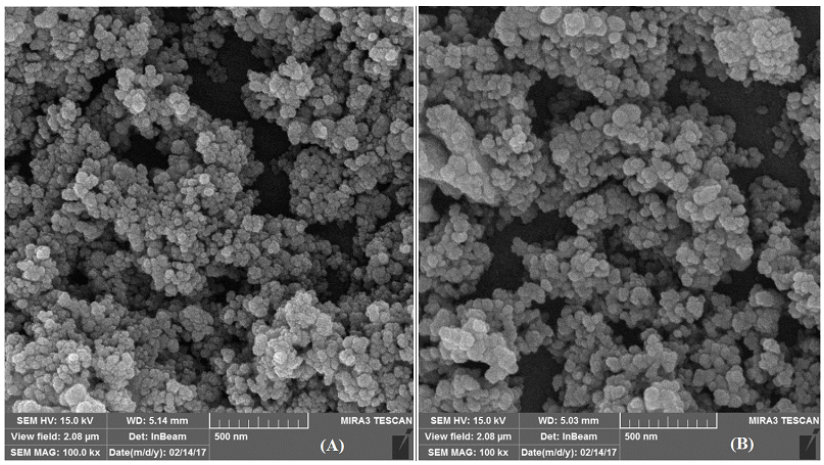

Figure 1 SEM images of the synthesized nano-sized NPs of (a) Fe_2O_3, and (b) Pb_3O_4

Characterization of the prepared metal oxides NPs by the XRD technique was carried out and as seen in Figure 2, XRD patterns of both samples show relatively intense diffraction peaks due to the formation of the targeted oxide products as the pure crystalline form compounds. The appeared peaks in Figure 2a are well-matched with the crystalline structure of α-Fe_2O_3 (JCPDS No 01-073-2234), while the ones shown in Figure 2b are consisted with the XRD pattern of Pb_3O_4 (PDF card No. 01-041-1493).

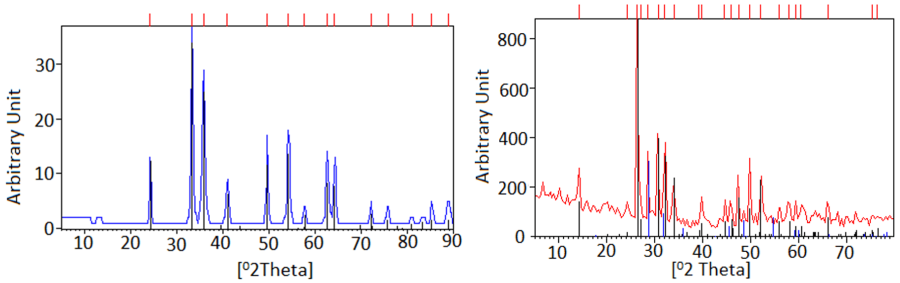

Figure 2 XRD patterns of the synthesized nano-sized NPs of (a) Fe_2O_3, and (b) Pb_3O_4

3.2 Characterization of the organized AP nano-composites

The made-up nano-composites of AP+Pb_3O_4 and AP+Fe_2O_3/Pb_3O_4 have dissimilar amounts of the nano-catalysts. These samples were inspected by SEM to describe their structure and morphology. SEM imageries of the inspected nano-composite samples are displayed in Figure 3, while SEM pictures of AP+Fe_2O_3/Pb_3O_4 nano-composites with 0.5, 2 and 5% content of Fe_2O_3/Pb_3O_4 NPs are specified in Figs 3a-c. These images illustrate that the morphology of AP particles in all samples is similar, whereas AP particles are formed as micron-sized pieces without extensive agglomeration.

The SEM imageries of the AP+Pb_3O_4 nano-composite samples containing 0.5, 2 and 5% of Pb_3O_4 NPs are specified in Figs 3 d-f, while these images evidently illustrate that Pb_3O_4 NPs are dispersed through the micron-sized AP particles with little agglomeration.

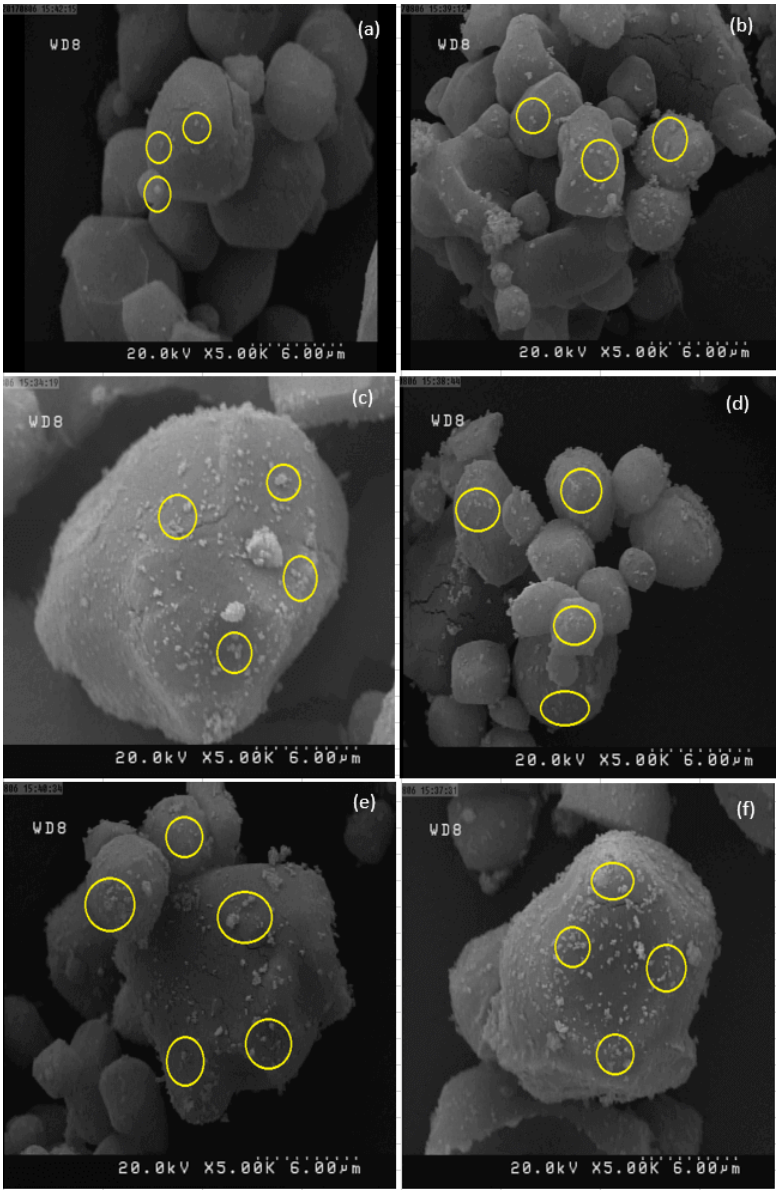

Figure 3 SEM images of AP+Fe_2O_3/Pb_3O_4 and AP+Pb_3O_4nano-composites: (a) AP+0.5% Fe_2O_3/Pb_3O_4; (b) AP+2% Fe_2O_3/Pb_3O_4; (c) AP+5% Fe_2O_3/Pb_3O_4; (d) AP+0.5% Pb_3O_4; (e) AP+2% Pb_3O_4 and (f) AP+5% Pb_3O_4.

3.3 Exploring catalytic activity of Fe_2O_3+Pb_3O_4 and Pb_3O_4 NPs in AP thermal decomposition

Thermal behavior of pure AP particles and prepared nano-composites was inspected by TG and DSC systems. Figure 4 gives DSC thermograms of these samples and correlated TG curves are exposed in Figure 5.

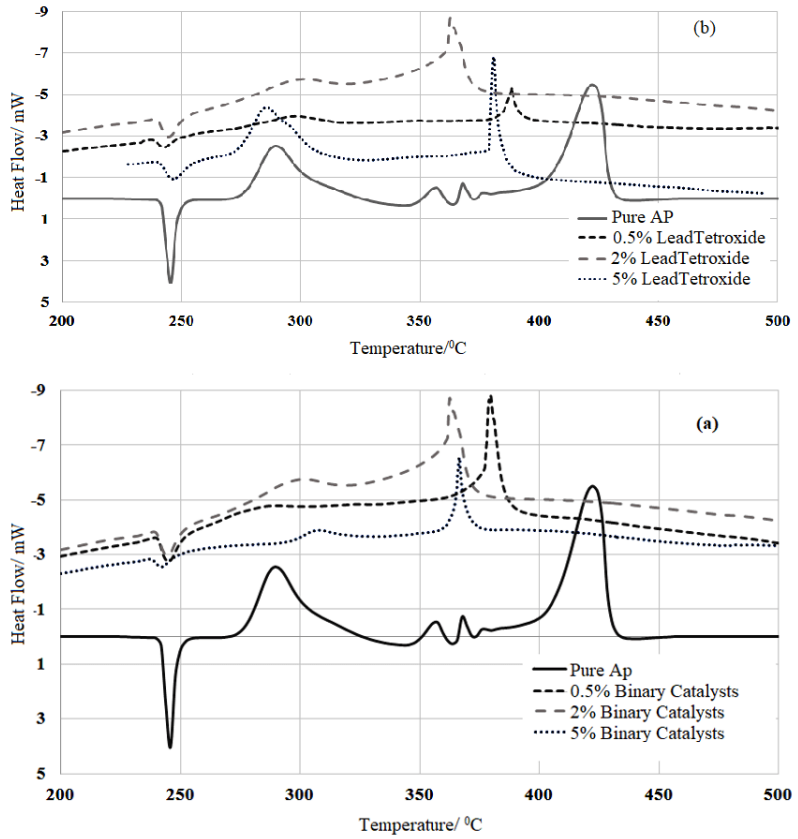

Figure 4 DSC curves of (a) pure AP and AP nano-composites in the presence of 0.5% Fe_2O_3/Pb_3O_4, 2% Fe_2O_3/Pb_3O_4 and 5% Fe_2O_3/Pb_3O_4 NPs and (b) pure AP and AP nano-composites in the presence of 0.5% Pb_3O_4, 2%+ Pb_3O_4 and 5%+ Pb_3O_4 NPs. Sample mass 3.0 mg; heating rate $10°C.min^{-1}$ and nitrogen atmosphere.

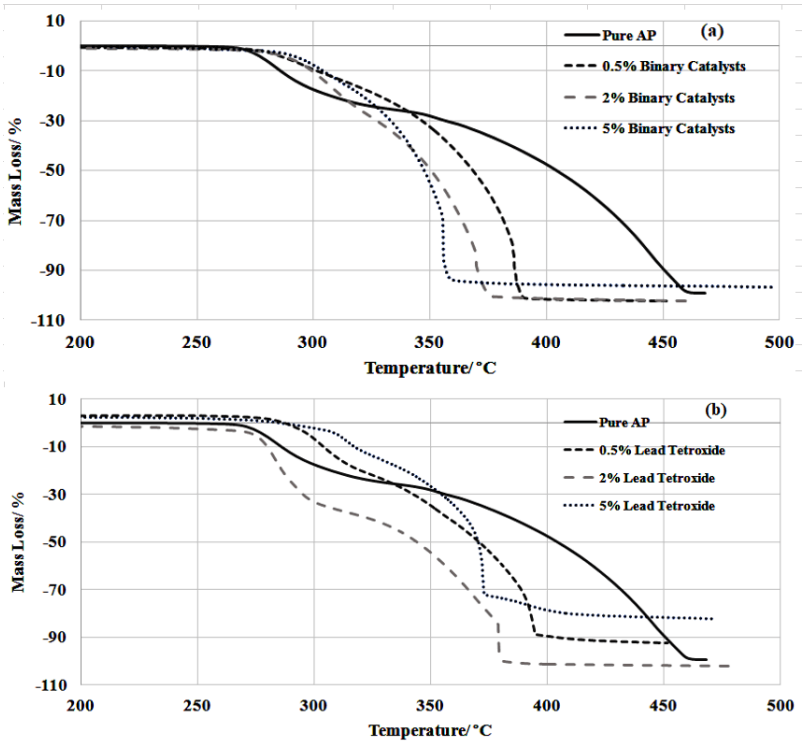

Figure 5 TG curves of (a) pure AP and AP nano-composites in the presence of 0.5% Fe_2O_3/Pb_3O_4, 2% Fe_2O_3/Pb_3O_4 and 5% Fe_2O_3/Pb_3O_4 NPs and (b) pure AP and AP nano-composites in the presence of 0.5% Pb_3O_4, 2%+ Pb_3O_4 and 5%+ Pb_3O_4 NPs. Sample mass 3.0 mg; heating rate $10°C.min^{-1}$ and nitrogen atmosphere.

DSC curve of pure AP (see Figure 4) shows three consecutive peaks which are obvious thru thermal decomposition pattern of this oxidant. The primary occurrence is appeared at 245.1°C as an endotherm while it is ascribed to the phase transition of AP crystal from orthorhombic to the cubic form [33]. Two other peaks which occurred at higher temperatures are exothermic, whereas the foremost is ostensible at 289.8 °C consistent to the primary decomposition of the pure AP. The consequent occasion is sensed as an exothermic peak at 421.7 °C, which is accountable for the decomposition of the formed intermediate in the previous step to the gassy products [34]. This trend defined for the pure AP decomposition is compatible with the TG thermogram (shown in Figure 4). The TG curve involves two individual mass losses through AP decomposition, whereas the earliest is accompanied by about 35.3±0.1% decline in the mass of sample and the second which occurred at a higher temperature shows about 64.7±0.1% mass loss. This trend is approved with the prior information published in the literature [34–36].

As seen in the Figure 4a, DSC curves of the AP nano-composites incorporating 0.5, 2 and 5% Fe_2O_3+Pb_3O_4 NPs are surprising and shows effective catalytic activities of the mixed NPs on thermal pattern of AP decomposition. In these samples in comparison with the pure AP, the endotherm event accountable for the phase conversion of AP crystals (˜245 °C) presented some slight modifications (reliant on their catalyst content) to the upper or lesser temperatures. Besides, in the presence of Fe_2O_3+Pb_3O_4 Nano-mixtures as the catalysts, both thermal decomposition peaks of AP show remarkable modification respect to the pure AP. Actually, Figure 4a shows that DSC curves of the AP nano-composites in the presence of Fe_2O_3+Pb_3O_4 NPs have a higher temperature at the first stage of dual decomposition events and this augmentation is further for the composite containing higher content of Fe_2O_3+Pb_3O_4NPs mixture. Conversely, these mixtures of NPs decline the temperature of the second step of AP decomposition and again this decline is reliant on the Fe_2O_3+Pb_3O_4 content of sample. Thermal patterns of AP nano-composites improved by Fe_2O_3+Pb_3O_4 NPs mixture in relating to the pure AP reveals that adding 0.5%, 2% and 5% mixture of Fe_2O_3+Pb_3O_4 NPs to the AP composition diminutions the temperature of subsequent stage of AP decomposition correspondingly nearby 42.0, 59.1 and 70.7 °C. Actually, announcing mix of Fe_2O_3+Pb_3O_4 NPs to the AP triggered plummeting the intermission temperature of the exothermic periods of decomposition and supports the combination of both events into solitary (Figure 4a). As could be seen in Figure 5a, TG curves of the AP nano-composites modified with the mix of Fe_2O_3+Pb_3O_4 NPs shows that addition of Fe_2O_3+Pb_3O_4 NPs mixture to the AP composition caused a remarkable declining in the temperature of AP decomposition at the final stage. Equally, mass loss accredited to decay of the AP in the presence of Fe_2O_3+Pb_3O_4 NPs mixture take places in a solitary stage compare to the pure AP. Similarly, AP nano-composites containing Fe_2O_3+Pb_3O_4 mixed NPs have surplus heat of decomposition. Figure 6 documents assessment of this item for the AP nano-composites and pure AP samples. As seen in this figure, the decomposition heat is enhances correspondingly for the pure AP, 0.5% Fe_2O_3+Pb_3O_4/AP, 2% Fe_2O_3+Pb_3O_4/AP and 5% Fe_2O_3+Pb_3O_4/AP to 880, 907, 1012 and 1165 $J.g^{-1}$.

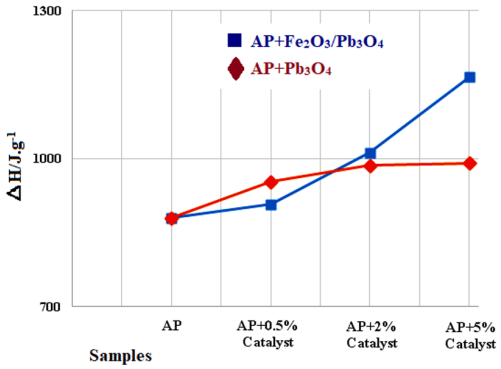

Figure 6 Effect of nano-catalysts (Fe_2O_3/Pb_3O_4 and Pb_3O_4) content on the heat of decomposition of nano-composites

Figs. 4b and 5b represent thermal curves of AP nano-composites modified with diverse amounts of Pb_3O_4 NPs inspected by DSC/TG systems. These curves clearly display the catalytic activity of the Pb_3O_4 NPs during thermal decomposition of the AP particles. As seen, Pb_3O_4 NPs has no substantial consequence on the phase transition of the AP particles and this endothermic event performs at similar temperature to that pure AP (˜245 °C). Unlike the pure AP, introducing Pb_3O_4 NPs to the AP composition drops the decomposition temperature of both stages of AP decay remarkably.

Figure 4b shows DSC curves of AP nano-composites modified with Pb_3O_4 NPs which approve

the effectual discount of AP decomposition temperature as a result of the catalytic role of Pb_3O_4 NPs. Decomposition temperature of the AP at the second period was abridged correspondingly nearby 33.2, 40.9 and 35.2 °C in the presence of 0.5%, 2% and 5% Pb_3O_4 NPs in comparison with the pure AP sample. Thermal pattern of AP particles in the presence of Pb_3O_4 NPs similar to mixed nano-catalyst improves by discount of the temperature interval amongst primary and subsequent stages of AP decomposition (Figure 4b). Provisionally, TG thermograms of the pure AP and AP nano-composites modified with Pb_3O_4 given in Figure 5a show that adding of Pb_3O_4 NPs to the AP composition triggered dropping of decomposition temperature of AP at the final stage of decay. Correspondingly, decay of AP nano-composites treated with Pb_3O_4 NPs divergence to the pure AP take places during a single stage. Furthermore, adding Pb_3O_4 NPs to the AP composition raised up the decomposition heat of AP. Figure 6 approves that adding of 0.5%, 2% and 5% Pb_3O_4NPs enhances decomposition heat of AP correspondingly to around 953, 986 and 991 J.g^{-1} related to the pure AP (880 J.g^{-1}).

3.4 Comparison catalytic activity of Fe_2O_3+Pb_3O_4 mixture with Pb_3O_4 NPs

Thermal decomposition of AP composition normally is carried out thru three individual periods including an endothermic and two exothermic occasions. The endotherm is outstanding to the phase transferring from orthorhombic to the cubic form of AP which happened at a temperature inferior than 250 °C. Next exothermic phases occurred at greater temperatures outstanding to the AP composition decay [37, 38]. Two miscellaneous mechanisms in the literature has been suggested for the thermal decay of AP composition [39–45]. One of these mechanisms is constructed the electron conveying from anion (*i.e.*, perchlorate) to cation to (*i.e.*, ammonium), and another is recognized by proton moving from cation (*i.e.*, ammonium) to the anion (*i.e.*, the perchlorate). Metal oxides catalytic role (*i.e.*, Fe_2O_3 and Pb_3O_4) in thermal decay of AP composition is reliant on this mechanism where the metal oxide might acts as the bridge for the electron-transformation. Consequently, Fe_2O_3 and Pb_3O_4 as two metal oxides as the catalysts may accelerate this process [41, 42].

Comparison of thermal patterns of AP nano-composites comprising of the mixed Fe_2O_3+Pb_3O_4 NPs and Pb_3O_4 NPs provides some interesting outcomes about their catalytic accomplishments. Thermal data about impact of the type and percentage of NPs on thermal behaviors of the AP samples are abridged in Table 1 which shows the type and amounts of NPs influence remarkably on the thermal decay of the AP composition.

TG curves of the pure AP delivers two individual decay stages with nearby 35.4% and 64.6% mass loose thru these periods. Nevertheless, TG curves of the AP nano-composites treated with Fe_2O_3/Pb_3O_4 NPs demonstrates robust catalytic role of the mixed NPs during decay of AP composition. Nonetheless, announcing of 5% mixture of Fe_2O_3+Pb_3O_4 NPs to the AP composition harvests improved outcomes than two other examined amounts (*i.e.*, 0.5 and 2%) in discount of the decay temperature of AP at the final period and rise of the AP heat of decomposition.

Also, TG curves of AP nano-composites modified with Pb_3O_4 NPs recognized the significant impact of Pb_3O_4 NPs on improving the thermal pattern of AP composition, though adding of 2% Pb_3O_4 NP to the AP showed a more outcome in thermal stability of the AP rather than two other contents. This improvement comprised further deteriorating of decay temperature of the AP composition at the ending period and additional augmentation of the decomposition heat.

Table 1 Effect of catalytic activity of Fe_2O_3/Pb_3O_4 and Pb_3O_4 NPs on the temperature and heat of decomposition of treated ammonium perchlorate particles

Sample No.	Composition	Thermal temperature/°C			ΔH/J.g-1
		Phase trans.	First event	Second event	
AP0	Pure AP	245.1	289.8	421.7	880
AP1	AP+0.5%Fe_2O_3/Pb_3O_4	244.8	-	379.7	907
AP2	AP+2% Fe_2O_3/Pb_3O_4	244.6	-	362.6	1012
AP3	AP+5% Fe_2O_3/Pb_3O_4	244.1	-	351	1165
AP4	AP+0.5% Pb_3O_4	242.7	-	388.5	953
AP6	AP+2% Pb_3O_4	243.6	-	380.8	986
AP7	AP+5% Pb_3O_4	241.7	-	386.5	991

The following explanations could be clarified the reducing decomposition temperature and enhancing the decomposition heat in the nano-composite particles (modified AP composition with the nano-catalysts):

First, increasing the efficient adsorption of the gaseous that produces during nano-composite decomposition (in compare to the pure AP decomposition), which consequently increases the gassy reaction [45].

Second, sputtering of the nano-composite particles during their thermal decomposition is less due to the higher surface area of NPs. Accordingly, this causes less mechanical loss and as a result their heat transference is performed more efficiently [45].

The thermos-kinetic parameters of the decomposition process might be obtained using thermal analysis outcomes by the aid of diverse approaches [46–48]. In this research, two eminent approaches were utilized to compute the Arrhenius factors (namely activation energy (E_a) and the frequency factor (A)) stand for the thermal decomposition of two AP nano-composites containing 5% Fe_2O_3/Pb_3O_4 and 2% Pb_3O_4 as the nano-composites which exhibited the best decomposition patterns. The calculation process was based on the DSC data of these nano-composite (Table 2) obtained under diverse heating rates. The Kissinger manner was the primary employed method in this research [49, 50]:

$$ln\frac{\beta}{T_m^2} = \ln\frac{AR}{E} - \frac{E}{RT_m} \quad (1)$$

In the$\ln\frac{\beta}{T_m^2} = \ln\frac{AR}{E} - \frac{E}{RT_m}$ formula, symbols R, β, T_m, and correspondingly signify the general gas constant, DSC heating rate, and the maximum peak temperature. In this approach, Ln ($\beta.{T_m}^{-2}$) is drawn against $1/T_m$ while the value of decomposition reaction activation energy is acquired from the slope of the occasioned linear line. The subsequent method developed in this work for figuring the Arrhenius factors of AP nano-composites was Starink [50, 51]:

$$Ln(\beta/{T_m}^{1.92}) + 1.0008E_a/RT_m = C \quad (2)$$

Maximum peak temperatures (T_m) for all inspected samples at various heating rates (β) of DSC as the input data for both methods are abbreviated in Table 2.

Table 2 The effect of heating rate on the maximum temperature (T_m) of decomposition of pure AP, AP+5% Fe_2O_3/Pb_3O_4 and AP+2% Pb_3O_4 nano-composites

Heating rate (β)/°C.min^{-1}	Pure AP/°C	AP+5%Fe_2O_3/Pb_3O_4/°C	AP+2% Pb_3O_4/°C
5	413.1	341	369.4
10	421.7	351	380.8
15	427.9	356.4	387.3
20	432.1	359.5	392.8

In Kissinger approach drawing Ln ($\beta{T_m}^{-2}$) versus $1/T_m$ yields the lines for the pure AP, AP/ 5% Fe_2O_3+Pb_3O_4 and AP/ 2% Pb_3O_4 with the regression coefficients (r) 0.9969, 0.9969 and, 0.9994, respectively (Table 3).

Table 3 Comparison of kinetic parameters for decomposition reaction of pure and treated ammonium perchlorate particles (AP+2% Pb_3O_4 & AP+5% Fe_2O_3/Pb_3O_4)

Samples	Pure AP		AP+5%Fe_2O_3/Pb_3O_4		AP+2% Pb_3O_4	
Parameter	Kissinger	Starink	Kissinger	Starink	Kissinger	Starink
E_a/ kJ mol^{-1}	280.3	280.6	226.7	227.1	201.4	201.8
log A	16.2	16.4	15.8	16.1	12.8	13.1
$\Delta G^{\neq}$/kJ mol^{-1}	240.5	237.2	194.3	191.6	205	202.2
$\Delta H^{\neq}$/kJ mol^{-1}	274.6	274.8	221.5	221.9	196	196.4
$\Delta S^{\neq}$/J mol^{-1} K^{-1}	49.1	54.1	43.6	48.6	-13.8	-8.9
r	0.9969	0.9969	0.9969	0.9969	0.9994	0.9994

Consideration of these results stipulates that the thermal decay mechanism of pure and nano-composites of AP is persistent at the established temperature range. According to the Kissinger equation, he slopes of the lines are equivalent to -E_a/R, henceforth, the values of activation energy (E_a) for the explored samples were found and the results are given in Table 3.

The activation energy (E_a) of the inspected samples by Starink methodology [50, 51] was calculated by drawing Ln ($\beta/{T_m}^{1.92}$) contrary to the inverse of maximum peak temperature. The outcomes for the pure AP, AP/ 5% Fe_2O_3+Pb_3O_4 and AP/ 2% Pb_3O_4 samples were correspondingly the lines with regression coefficients (r) 0.9969, 0.9969 and 0.9994. Then, the activation energy (E_a) values for the inspected samples were computed from their slopes according the methodology and the results are demonstrated in Table 3.

Successively, frequency factor values (A) for the inspected samples were calculated using the subsequent formulary prearranged by ASTM E698 [52]:

$$A = \beta\left(\frac{E_a}{RT_m^2}\right)\exp\left(\frac{E_a}{RT_m}\right) \quad (3)$$

Frequency factor (A) values computed by means of the equation (5) are demonstrated in Table 3. Comparing the obtained values of kinetic factors for the inspected samples by both methods

proven that both methodologies spectacle comparable trend and proposed analogous values for the activation energies of the inspected samples. Correspondingly, thermodynamic issues associated with the activation of the decay reaction might be attained using of the succeeding equations [53–55]:

$$A \exp \frac{-E}{RT} = \nu \exp \frac{-\Delta G^{\neq}}{RT} \tag{4}$$

$$\Delta H^{\neq} = E - RT \tag{5}$$

$$\Delta G^{\neq} = \Delta H^{\neq} - T\Delta S^{\neq} \tag{6}$$

In these $\Delta S^{\#}$, $\Delta G^{\#}$, and $\Delta H^{\#}$ one-to-one denotes the entropy, the Gibbs free energy, and the enthalpy of the decay activation. In addition, υ=$K_B T/h$ (h and K_B correspondingly denote the Plank and Boltzmann constants). The premeditated values of the kinetic and the thermodynamic issues are represented in Table 3 for the pure AP and 5% Fe_2O_3+Pb_3O_4 and 2% Pb_3O_4 nano-composites of AP. The outcomes establish that introducing of Pb_3O_4 or mixture of Fe_2O_3+Pb_3O_4 NPs to AP composition triggered an extensive reduction in the values of E_a, $\Delta H^{\#}$ and $\Delta S^{\#}$ responsible for thermal decay of the AP samples. Additionally, adding 5% mix of Fe_2O_3+Pb_3O_4 or 2% Pb_3O_4 NPs to AP composition lessen $E_a$values correspondingly to about 226.7 and 201.4 $kJmol^{-1}$, which is close to 60% and 50% of E_a for pure AP. Table 3 demonstrates that others activation issues appearance similar trend for the nano-composites respect to pure AP.

Table 4 A simple benchmark of Catalytic activities of different NPs on the thermal decomposition of the ammonium perchlorate

Composition	Thermal temperature/ °C of second peak	ΔH /J.g^{-1}	Refrences
Pure AP	421.7	880	
AP+Fe_2O_3/Pb_3O_4	351	1165	Current Research
AP+ Pb_3O_4	380.8	986	
AP+MgO	317.2	1588	[56]
AP+ZnO	350.4	1590	
AP+CuO	354.8	1512	[57]
AP+La_2O_3	317.2	1588	
AP+$LaFeO_3$	374	1030	
AP+$LaNiO_3$	377	1090	[58]
AP+$LaCoO_3$	–	1470	
AP+Cr_2O_3	373	–	[59]
AP+Fe_2O_3	343	–	

Table 4 has been prepared for a simple comparison. The table shows the efficiency of lead and iron metal oxides compared to other metal oxides used in the decomposition of ammonium perchlorate.

4 Conclusion

Fe_2O_3 and Pb_3O_4 NPs were profitably made-up by the calcinations of their precursors in the form of carbonate salt. The fabricated NPs were characterized by XRD and SEM approaches to analysis their structure and morphology. Their results documented formation of Fe_2O_3 and Pb_3O_4 NPs, while they possess respectively the average particle sizes near 40 and 46 nm. Synthesized NPs were utilized in the composition of AP as nano-catalysts, while their catalytic behaviors in the AP composites were tested by thermal methods. Results of thermal analysis were unexpected, though demonstrated the strong catalytic effects of NPs by substantial drop in the AP decomposition temperature, and augmentation of the decomposition heat of AP. Moreover, the findings of the present work disclosed that presence of NPs (either Fe_2O_3+Pb_3O_4 or pure Pb_3O_4) prominently decreases E_a, $\Delta H^{\neq}$ and $\Delta S^{\neq}$ of AP than the pure AP.

Conflict of interest

The authors declare that there is no conflict of interest.

References

[1] Rajić M and Sućeska M. Study of thermal decomposition kinetics of low-temperature reaction of ammonium perchlorate by isothermal TG. Journal of Thermal Analysis and Calorimetry, 2000, **63**(2): 375-386.
https://doi.org/10.1023/A:1010136308310

[2] Zhi J, Tian-Fang W, Shu-Fen L, *et al*. Thermal behavior of ammonium perchlorate and metal powders of different grades. Journal of Thermal Analysis and Calorimetry, 2006, **85**(2): 315-320. https://doi.org/10.1007/s10973-005-7035-7

[3] Farhadian AH, Tehrani MK, Keshavarz MH, *et al*. A novel approach for investigation of chemical aging in composite propellants through laser-induced breakdown spectroscopy (LIBS). Journal of Thermal Analysis and Calorimetry, 2016, **124**(1): 279-286. https://doi.org/10.1007/s10973-015-5116-9

[4] Shamsipur M, Pourmortazavi SM, Roushani M, *et al*. Thermal behavior and non-isothermal kinetic studies on titanium hydride-fueled binary pyrotechnic compositions. Combustion Science and Technology, 2013, **185**: 122-133. https://doi.org/10.1080/00102202.2012.70956

[5] Mezroua A, Khimeche K, Lefebvre MH, *et al*. The influence of porosity of ammonium perchlorate (AP) on the thermomechanical and thermal properties of the AP/ polyvinylchloride (PVC) composite propellants. Journal of Thermal Analysis and Calorimetry, 2014, **116**(1): 279-286. https://doi.org/10.1007/s10973-013-3517-1

[6] Trache D, Maggi F, Palmucci I, *et al*. Effect of amide-based compounds on the combustion characteristics of composite solid rocket propellants. Arabian Journal of Chemistry, 2019, **12**(8): 3639-3651. https://doi:10.1016/j.arabjc.2015.11.016

[7] Patil PR, Krishnamurthy VE and Joshi SS. Effect of nano-copper oxide and copper chromite on the thermal decomposition of ammonium perchlorate. Propellants Explosives Pyrotechnics, 2008, **33**(4): 266-270. https://doi.org/10.1002/prep.200700242

[8] Wang Y, Zhu J, Yang X, *et al*. Preparation of NiO nanoparticles and their catalytic activity in the thermal decomposition of ammonium perchlorate. Thermochima Acta, 2005, **437**(1): 106-109. https://doi.org/10.1016/j.tca.2005.06.027

[9] Pourmortazavi SM, Rahimi-Nasrabadi M, Rai H, *et al*. Role of metal oxide nanomaterials on thermal stability of 1,3,6-trinitrocarbazole. Propellants Explosives Pyrotechnics, 2016, **41**: 912-918. https://doi.org/10.1002/prep.201500312

[10] Hosseini SG, Toloti SJ, Babaei K, *et al*. The effect of average particle size of nano-Co3O4 on the catalytic thermal decomposition of ammonium perchlorate particles. Journal of Thermal Analysis and Calorimetry, 2016, **124**(3): 1243-1254. https://doi.org/10.1007/s10973-016-5333-x

[11] Pourmortazavi SM, Rahimi-Nasrabadi M, Rai H, *et al*. Effect of Nanomaterials on Thermal Stability of 1,3,6,8-Tetranitro Carbazole. Central European Journal of Energetic Materials, 2017, **14**: 201-216. https://doi.org/10.22211/cejem/65140

[12] Yin JZ, Lu QY, Yu ZN, *et al*. Hierarchical ZnO nanorod-assembled hollow superstructures for catalytic and photoluminescence applications. Crystal Growth & Design, 2010, **10**(1): 40-43. https://doi.org/10.1021/cg901200u

[13] Sun X, Qiu X, Li L, *et al*. ZnO twin-cones: synthesis, photoluminescence, and catalytic decomposition of ammonium perchlorate. Inorganic Chemistry, 2008, **47**(10): 4146-4152. https://doi.org/10.1021/ic702348c

[14] Zhao S and Ma D. Preparation of CoFe2O4 nanocrystallites by solvothermal process and its catalytic activity on the thermal decomposition of ammonium perchlorate. Journal of Nanomaterials, 2010, 48-53. https://doi.org/10.1155/2010/842816

[15] Aijun H, Juanjuan L, Mingquan Y, *et al*. Preparation of nano-MnFe2O4 and its catalytic performance of thermal decomposition of ammonium perchlorate. Chinese Journal of Chemical Engineering, 2011, **19**(6): 1047-1051. https://doi.org/10.1016/S1004-9541(11)60090-6

[16] Singh G, Kapoor I and Dubey S. Nanocobaltite: preparation, characterization, and their catalytic activity. Propellants Explosives Pyrotechnics, 2011, **36**(4): 367-372. https://doi.org/10.1002/prep.201000040

[17] Chen L, Li L and Li G. Synthesis of CuO nanorods and their catalytic activity in the thermal decomposition of ammonium perchlorate. Journal of Alloys and Compounds, 2008, **464**(1-2): 532-536. https://doi.org/10.1016/j.jallcom.2007.10.058

[18] Matijevic E. Preparation and properties of uniform size colloids. Chemistry of Materials, 1993, **5**: 412-426. https://doi.org/10.1021/cm00028a004

[19] Ozin GA. Nonochemistry: Synthesis in diminishing dimensions, Advanced Materials, 1992, **4**: 612-649. https://doi.org/10.1002/adma.19920041003

[20] Furstner A. Active Metals: Preparation, Characterization, Applications. Weinheim, New York, VCH, 1996.

[21] Shekhah O, Ranke W, Schule A, *et al*. Styrene Synthesis: High Conversion over Unpromoted Iron Oxide Catalysts under Practical Working Conditions. Angewandte Chemie International Edition, 2003, **42**(46): 5760-5763. https://doi.org/10.1002/anie.200352135

[22] Gondal MA, Hameed A, Yamani ZH, *et al*. Production of hydrogen and oxygen by water splitting using laser induced photo-catalysis over Fe2O3. Applied Catalysis A: General, 2004, **268**(1-2): 159-167. https://doi.org/10.1016/j.apcata.2004.03.030

[23] Li P, Miser DE, Rabiei S, *et al*. Hajaligol, The removal of carbon monoxide by iron oxide nanoparticles. Applied Catalysis B: Environmental, 2003, **43**(2): 151-162. https://doi.org/10.1016/S0926-3373(02)00297-7

[24] Fabrizioli P, Burgi T and Baiker A. Environmental Catalysis on Iron Oxide–Silica Aerogels: Selective Oxidation of NH3 and Reduction of NO by NH3. Journal of Catalysis, 2002, **206**(1): 143-154. https://doi.org/10.1006/jcat.2001.3475

[25] Lauwiner M, Rys P and Wissmann J. Reduction of Aromatic Nitro Compounds with Hydrazine Hydrate in the Presence of an Iron Oxide Hydroxide Catalyst. I. The Reduction of Monosubstituted Nitrobenzenes with Hydrazine Hydrate in the Presence of ferrihydrite. Applied Catalysis A: General, 1998, **172**: 141-148. https://doi.org/10.1016/S0926-860X(98)00110-0

[26] Xu H, Wang X and Zhang L. Selective preparation of nanorods and micro-octahedrons of Fe2O3 and their catalytic performances for thermal decomposition of ammonium perchlorate. Powder Technology, 2008, **185**: 176-180. https://doi.org/10.1016/j.powtec.2007.10.011

[27] Joshi SS, Patil PR and Krishnamurthy VN. Thermal Decomposition of Ammonium Perchlorate in the Presence of Nanosized Ferric Oxide. Defence Science Journal, 2008, **58**(6): 721-727.

[28] Arami H, Mazloumi M, Khalifehzadeh R, *et al*. Surfactant free hydrothermal formation of Pb3O4 nanorods. Journal of Alloys & Compounds, 2008, **466**: 323-325. https://doi.org/10.1016/j.jallcom.2007.11.027

[29] Sellin PJ. Thick film compound semiconductors for X-ray imaging applications. Nuclear Instruments & Methods in Physics Research, 2006, **563**: 1-8. https://doi.org/10.1016/j.nima.2006.01.110

[30] Raviendra D. Transparent conducting PbO2 films prepared by activated reactive evaporation. Physical Review B, 1986, 33(4): 2660-2664. https://doi.org/10.1103/physrevb.33.2660

[31] Sljukic B, Banks CE, Crossley A, *et al*. Lead(IV) oxide-graphite composite electrodes: application to sensing of ammonia, nitrite, and phenols. Analytica Chimica Acta, 2007, **587**(2): 240-246. https://doi.org/10.1016/j.aca.2007.01.041

[32] Abusaidi H, Ghaieni HR, Pourmortazavi SM, *et al*. Effect of nitro content on thermal stability and decomposition kinetics of nitro-HTPB. Journal of Thermal Analysis and Calorimetry, 2016, **124**: 935-941. https://doi.org/10.1007/s10973-015-5178-8

[33] Hosseini SG, Abazari R and Gavi A. Pure CuCr2O4 nano particles: Synthesis, characterization and their morphological and size effects on the catalytic thermal decomposition of ammonium perchlorate. Solid State Science, 2014, **37**: 72-79. https://doi.org/10.1016/j.solidstatesciences.2014.08.014

[34] Zhang WJ, Li P, Xu HB, *et al*. Thermal decomposition of ammonium perchlorate in the presence of Al(OH)3.Cr(OH)3 nano particles. Journal of Hazard Materials, 2014, **268**: 273-80. https://doi.org/10.1016/j.jhazmat.2014.01.016

[35] Rajić M and Sućeska M. Study of Thermal Decomposition Kinetics of Low-temperature Reaction of Ammonium Perchlorate by Isothermal TG. Journal of Thermal Analysis and Calorimetry, 2000, **63**: 375-386. https://doi.org/10.1023/A:1010136308310

[36] Zhi J, Tian-Fang W, Shu-Fen L, *et al*. Thermal behavior of ammonium perchlorate and metal powders of different grades. Journal of Thermal Analysis and Calorimetry, 2006, **85**: 315-320. https://doi.org/10.1007/s10973-005-7035-7

[37] Alizadeh-Gheshlaghi E, Shaabani B, Khodayari A, *et al*. Investigation of the catalytic activity of nano-sized CuO, Co3O4 and CuCo2O4 powders on thermal decomposition of ammonium perchlorate. Powder Technology, 2012, **217**: 330-339. https://doi.org/10.1016/j.powtec.2011.10.045

[38] Yang C, Wang J, Xiao F, *et al*. Microwave hydrothermal disassembly for evolution from CuO dendrites to nano sheets and their applications in catalysis and photo-catalysis. Powder Technology, 2014, **264**: 36-42. https://doi.org/10.1016/j.powtec.2014.05.012

[39] Wang J, He S, Li Z, *et al*. Self-assembled CuO nano architectures and their catalytic activity in the thermal decomposition of ammonium perchlorate. Colloid and Polymer Science, 2009, **287**: 853-858. https://doi.org/10.1007/s00396-009-2040-1

[40] Dubey BL, Singh NB, Srivastava JN, *et al*. The catalytic behavior of NiFe2-xCrxO4 during the thermal decomposition of ammonium perchlorate, polystyrene and their composite propellants. Indian Journal of Chemistry, 2001, **40**(8): 841-847.

[41] Freeman ES and Anderson DA. Effects of radiation and doping on the catalytic activity of magnesium oxide on the thermal decomposition of potassium perchlorate. Nature, 1965, **206**: 378-379. https://doi.org/10.1038/206378a0

[42] Mirzajani V, Farhadi K and Pourmortazavi SM. Catalytic effect of lead oxide nano- and microparticles on thermal decomposition kinetics of energetic compositions containing TEGDN/NC/DAG. Journal of Thermal Analysis and Calorimetry, 2018, **131**: 937-48. https://doi.org/10.1007/s10973-017-6666-9

[43] Boldyrev VV. Thermal decomposition of ammonium perchlorate. Thermochimica Acta, 2006, **443**: 1-36. https://doi.org/10.1016/j.tca.2005.11.038

[44] Chen L, Li L and Li G. Synthesis of CuO nano rods and their catalytic activity in the thermal decomposition of ammonium perchlorate. Journal of Alloys & Compounds, 2008, **464**: 532-536. https://doi.org/10.1016/j.jallcom.2007.10.058

[45] Patil PR, Krishnamurthy VN and Joshi SS. Differential scanning calorimetric study of HTPB based composite propellants in presence of nano ferric oxide. Propellants, Explosives, Pyrotechnics, 2006, **31**: 442-426. https://doi.org/10.1002/prep.200600059

[46] Pourmortazavi SM, Rahimi-Nasrabadi M, Kohsari I, *et al*. Non-isothermal kinetic studies on thermal decomposition of energetic materials. Journal of Thermal Analysis and Calorimetry, 2012, **110**: 857-863. https://doi.org/10.1007/s10973-011-1845-6

[47] Eslami A and Hosseini SG. Improving safety performance of lactose-fueled binary pyrotechnic systems of smoke dyes. Journal of Thermal Analysis and Calorimetry, 2011, **104**: 671-678. https://doi.org/10.1007/s10973-010-1062-8

[48] Pourmortazavi SM, Sadri M, Rahimi-Nasrabadi M, *et al*. Thermal decomposition kinetics of electrospun azidodeoxy cellulose nitrate and polyurethane nanofibers. Journal of Thermal Analysis and Calorimetry, 2015, **119**: 281-290. https://doi.org/10.1007/s10973-014-4064-0

[49] Kissinger HE. Reaction kinetics in differential thermal analysis. Analytical Chemistry, 1957, **29**: 1702-1706. https://doi.org/10.1021/ac60131a045

[50] Pourmortazavi SM, Farhadi K, Mirzajani V, *et al*. Study on the catalytic effect of diaminoglyoxime on thermal behaviors, non-isothermal reaction kinetics and burning rate of homogeneous double-base propellant. Journal of Thermal Analysis and Calorimetry, 2016, **125**: 121-128. https://doi.org/10.1007/s10973-016-5373-2

[51] Starink MJ. The determination of activation energy from linear heating rate experiments: a comparison of the accuracy of iso conversion methods. Thermochimica Acta, 2003, **404**: 163-176. https://doi.org/10.1016/S0040-6031(03)00144-8

[52] ASTM E698-05. Standard test method for Arrhenius kinetic constants for thermally unstable materials. https://doi.org/10.1520/E0698-05

[53] Pourmortazavi SM, Mirzajani V and Farhadi K. Thermal behavior and thermokinetic of double-base propellant catalyzed with magnesium oxide nanoparticles. Journal of Thermal Analysis and Calorimetry, 2018, **173**: 1-12. https://doi.org/10.1007/s10973-018-7904-5

[54] Rocco J, Lima J, Frutuoso AG, *et al*. Studies of a composite solid rocket propellant based on HTPB-binder. Journal of Thermal Analysis and Calorimetry, 2004, **77**: 803-813. https://doi.org/10.1023/B:JTAN.0000041659.97749.fe

[55] Shamsipur M, Pourmortazavi SM, Hajimirsadeghi SS, *et al*. Effect of functional group on thermal stability of cellulose derivative energetic polymers. Fuel, 2012, 95: 394-399. https://doi.org/10.1016/j.fuel.2011.09.036

[56] MomenizadehPandas H and Fazli M. Fabrication of MgO and ZnO nanoparticles by the aid of eggshell bioactive memberane and exploring their catalytic activities on the thermal decomposition of ammounium perchlorate. Journal of Thermal Analysis & Calorimetry, 2018, **131**: 2913. https://doi.org/10.1007/s10973-017-6814-2

[57] MomenizadehPandas H and Fazli M.M. Preparation and Application of La2O3 and CuO Nano Particles as Catalysts for Ammonium Perchlorate Thermal Decomposition, Propellants, Explosives. Pyrotechnics, 2018, **43**: 1096. https://doi.org/10.1002/prep.201800036

[58] Wang Y, Yang X, Lu L, *et al*. Experimental study on preparation of LaMO3 (M = Fe, Co, Ni) nanocrystals and their catalytic activity. Thermochimica Acta, 2006, **433**(2): 225-230. https://doi.org/10.1016/j.tca.2006.01.030

[59] Kapoor IPS, Srivastava P and Singh G. Nanocrystalline Transition Metal Oxides as Catalysts in the Thermal Decomposition of Ammonium Perchlorate. Propellants, Explosives, Pyrotechnics, 2009, **34**: 351-356. https://doi.org/10.1002/prep.200800025